Electronic Supplementary Material (ESI) for Journal of Materials Chemistry C.
This journal is © The Royal Society of Chemistry

Electronic Supplementary Information

All-Fused-Ring Small Molecule Acceptors with Near-Infrared Absorption

Xiaoyu Zhu,[ab] Yongqian Zhang,[ab] Bomin Xie,[c] Junhui Miao,*[a] Wei Ma,*[c] Jun Liu*[ab] and Lixiang Wang[ab]

[a]State Key Laboratory of Polymer Physics and Chemistry, Changchun Institute of Applied Chemistry, Chinese Academy of Sciences, Changchun 130022, China.

[b]University of Science and Technology of China, Hefei 230026, China.

[c]State Key Laboratory for Mechanical Behavior of Materials, Xi'an Jiaotong University, Xi'an 710049, China.

E-mail: jhmiao@ciac.ac.cn; msewma@xjtu.edu.cn; liujun@ciac.ac.cn.

Contents

1. Experimental details

General. ^{1}H NMR and ^{13}C NMR spectra were measured with a Bruker AV-500 MHz NMR spectrometer at room temperature. Mass spectra were performed on a Bruker Daltonics Flex matrix-assisted laser desorption ionization time of flight mass spectrometer (MALDI-TOF-MS). The thermogravimetric analysis (TGA) was performed on a Perkin-Elmer 7 instrument at a heating rate of 10 ^{o}C min^{-1} under purified nitrogen gas (N_2) flow. The decomposition temperature (T_d) corresponded to 5% loss of weight. 2D grazing incidence wide angle X-ray scattering (2D-GIWAXS) were measured at the SAXS/WAXS beamline at Australian Synchrotron ANSTO. Samples of pure materials or blends were prepared on Silicon dioxide substrates. UV-vis absorption spectra (in CF solution and as thin films) were obtained with a Shimadzu UV-3600 spectrometer. Cyclic voltammogram (CV) measurements were performed on a CHI660a electrochemical workstation using glassy carbon as the working electrode, Pt wire as the counter electrode, and a standard calomel reference electrode in a 0.1 mol L^{-1} tetrabutylammonium hexafluorophosphate (Bu_4NPF_6) acetonitrile solution. The materials were casted on the working electrode for measurements and ferrocene as an internal reference at a scan rate of 100 mV s^{-1}. The highest occupied molecular orbital (HOMO) and the lowest unoccupied molecular orbital (LUMO) energy levels of the materials were estimated by the equations: $E_{HOMO/LUMO} = -(4.80 + E_{onset}^{ox}/E_{onset}^{red})$ eV. The AFM images were recorded using a SPA300HV (Seiko Instruments, Inc., Japan) in tapping mode. Photoluminescence (PL) spectra were measured with a Horiba Jobin-Yvon FL3C-111 fluorescence spectrophotometer. The pure and blend film samples were fabricated by spin-coating the CF solutions onto quartz substrates. The thickness of films was measured with a Dektak 6M Stylus Profilometer.

Reagents. Toluene was dried using sodium before use. Dichloromethane and *N,N*-dimethylacetamide were purchased from commercial sources and used as received.

2. Syntheses and characterizations

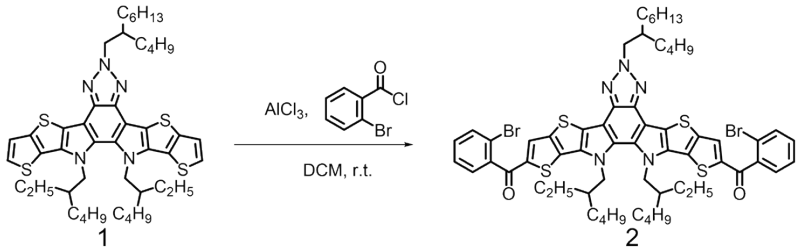

1 2

Compound 2: Under protection of argon, 2-Bromobenzoyl chloride (0.25 g, 1.15 mmol) and aluminum chloride (0.31 g, 2.31 mmol) were added to a solution of compound 1 (0.47 g, 0.58 mmol) in anhydrous dichloromethane (20.0 mL). The mixture was stirring at room temperature for 24 hours. Then the solution was quenched with water and extracted with CH_2Cl_2. The organic layer was washed with water and brine, and was dried over Na_2SO_4, after removal of solvent, this crude product was purified by silica gel chromatography (petroleum ether/dichloromethane = 1.5:1.0, v/v) to afford compound 2 (0.61 g, yield: 90%) as an orange solid. ^{1}H NMR (500 MHz, Chloroform-*d*) δ 7.72 (d, *J* = 8.0 Hz, 1H), 7.66 (s, 1H), 7.55 (d, *J* = 9.1 Hz, 1H), 7.48 (t, *J* = 7.5 Hz, 1H), 7.43 – 7.38 (m, 1H), 4.69 (d, *J* = 27.7 Hz, 3H), 2.37 (s, 0.5H), 2.05 – 1.85 (m, 1H), 1.38 – 1.18 (m, 8H), 1.05 – 0.78 (m, 11H), 0.72 – 0.49 (m, 6H). ^{13}C NMR (126 MHz, Chloroform-d) δ 187.74, 141.96, 141.09, 140.25, 136.79, 135.81, 133.51, 132.16, 131.92, 131.38, 130.64, 128.96, 127.22, 127.06, 119.73, 110.58, 77.29, 77.04, 76.78, 59.69, 54.90, 40.13, 38.99, 31.70, 31.37, 30.97, 29.51, 28.28, 27.38, 26.09, 23.19, 23.13, 23.13, 22.91, 22.66, 22.64, 22.59, 14.07, 14.01, 13.64, 13.63, 10.20, 10.10.

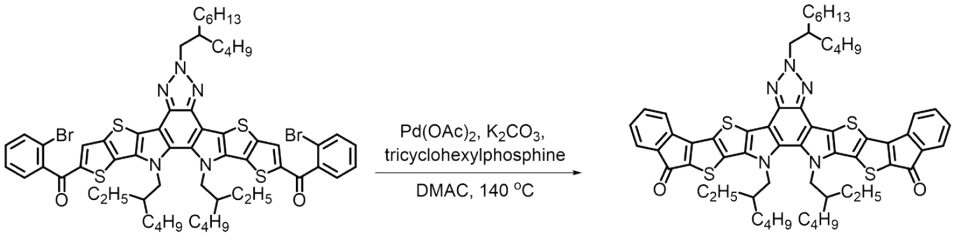

2 3

Compound 3: Under protection of argon, $Pd(OAc)_2$ (10 mg, 0.05 mmol), tricyclohexylphosphine (51 mg, 0.18 mmol), K_2CO_3 (249 mg, 1.81 mmol) was added to a solution of compound 2 (0.53 g, 0.45 mmol) in 40.0 mL *N,N*-dimethylacetamide. The mixture was heated to reflux overnight. Then the solution was poured into water and extracted with CH_2Cl_2, the organic layer was washed with water and brine, and was dried over Na_2SO_4, after removal of solvent, this crude product was purified by silica gel chromatography (petroleum ether/dichloromethane = 1.0:2.5, v/v) to afford

compound 3 (340 mg, yield: 74%) as a purple black solid. ^{1}H NMR (500 MHz, Chloroform-*d*) δ 7.55 (d, *J* = 7.1 Hz, 1H), 7.44 (t, *J* = 7.9 Hz, 1H), 7.34 (d, *J* = 7.1 Hz, 1H), 7.29 – 7.27 (m, 1H), 4.76 (d, *J* = 7.1 Hz, 1H), 4.61 (d, *J* = 7.8 Hz, 2H), 2.41 (s, 0.5H), 1.93 (m, *J* = 18.2 Hz, 1H), 1.36 – 1.27 (m, 8H), 0.92 – 0.82 (m, 11H), 0.71 – 0.50 (m, 6H). ^{13}C NMR (126 MHz, Chloroform-d) δ 185.26, 151.26, 138.30, 138.18, 136.81, 135.86, 135.78, 134.78, 133.34, 133.22, 132.28, 128.83, 127.27, 123.70, 120.08, 110.84, 77.27, 77.02, 76.76, 59.87, 55.05, 40.23, 39.06, 31.79, 31.43, 31.08, 29.59, 28.41, 26.12, 23.26, 22.93, 22.68, 14.13, 14.04, 13.65, 10.09.

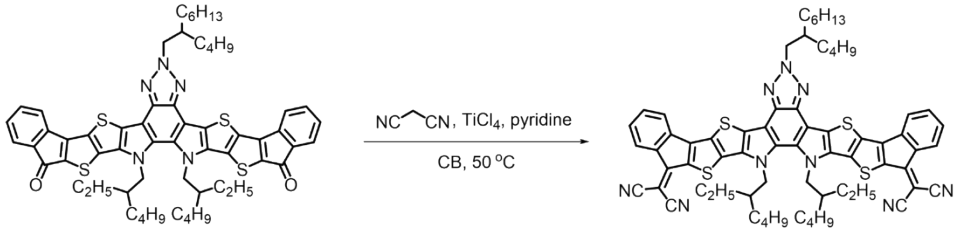

3 FM3

Compound FM3: To a stirred solution of compound 3 (172 mg, 0.17 mmol) and malononitrile (56 mg, 0.84 mmol) in 10.0 ml chlorobenzene was added 0.2 mL pyridine and 0.2 mL $TiCl_4$, the solution was heated to 50 °C for 4 hours. Then the solution was poured into water and extracted with CH_2Cl_2, the organic layer was washed with water and brine, and was dried over Na_2SO_4, after removal of solvent, this crude product was purified by silica gel chromatography (petroleum ether/dichloromethane = 1.0:3.0, v/v) to afford compound FM3 (140 mg, yield: 74%) as a black solid. ^{1}H NMR (500 MHz, Chloroform-*d*) δ 8.20 (d, *J* = 7.6 Hz, 1H), 7.44 (d, *J* = 6.9 Hz, 2H), 7.33 – 7.27 (m, 1H), 4.73 (d, *J* = 7.0 Hz, 1H), 4.62 (d, *J* = 7.5 Hz, 2H), 2.41 (s, 0.5H), 1.93 (m, *J* = 18.2 Hz, 1H), 1.36 – 1.27 (m, 8H), 0.92 – 0.82 (m, 11H), 0.71 – 0.50 (m, 6H). ^{13}C NMR (101 MHz, 1,2-Dichlorobenzene-d4) δ 156.46, 147.18, 138.67, 137.87, 137.15, 136.43, 133.54, 133.14, 132.45, 131.26, 130.91, 129.63, 128.49, 126.64, 125.92, 121.15, 114.31, 113.39, 112.34, 71.01, 60.26, 56.24, 41.12, 32.36, 31.96, 31.90, 30.60, 29.69, 28.93, 28.43, 26.68, 24.22, 23.00, 22.80, 13.96, 13.83, 13.50, 10.30. MS (MALDI-TOF): Calculated for $C_{66}H_{67}N_9S_2$ [M^+], 1113.4; found, 1113.4.

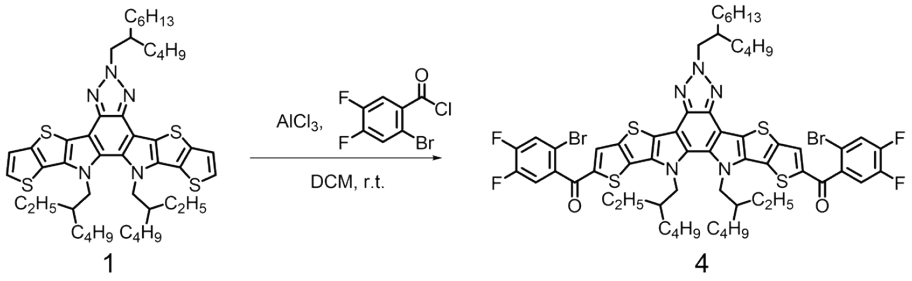

1 4

Compound 4: Under protection of argon, 2-bromo-4,5-difluorobenzoyl chloride (314 mg, 1.23 mmol) and aluminum chloride (164 mg, 1.23 mmol) were added to a solution of compound 1 (250 mg, 0.31 mmol) in anhydrous dichloromethane (8.0 mL). The mixture was stirring at room temperature for 24 hours. Then the solution was quenched with water and extracted with CH_2Cl_2. The organic layer was washed with water and brine, and was dried over Na_2SO_4, after removal of solvent, this crude product was purified by silica gel chromatography (petroleum ether/dichloromethane = 1.5:1.0, v/v) to afford compound 4 (283 mg, yield: 74%) as an orange solid. ^{1}H NMR (500 MHz, Chloroform-*d*) δ 7.69 (s, 1H), 7.62 –7.53 (m, 1H), 7.46 – 7.39 (m, 1H), 4.72 (d, *J* = 7.1 Hz, 1H), 4.65 (d, *J* = 7.7 Hz, 2H), 2.38 (s, 0.5H), 2.00 – 1.90 (m, 1H), 1.42 – 1.23 (m, 8H), 1.04 – 0.74 (m, 11H), 0.72 – 0.50 (m, 6H). ^{13}C NMR (126 MHz, Chloroform-d) δ 185.27, 148.35, 141.27, 140.99, 136.75, 135.80, 132.34, 132.31, 130.73, 127.58, 122.87, 122.71, 118.18, 118.02, 114.11, 110.75, 77.27, 77.02, 76.76, 59.76, 54.95, 40.18, 39.02, 31.39, 30.99, 29.46, 27.49, 27.40, 13.63, 10.10.

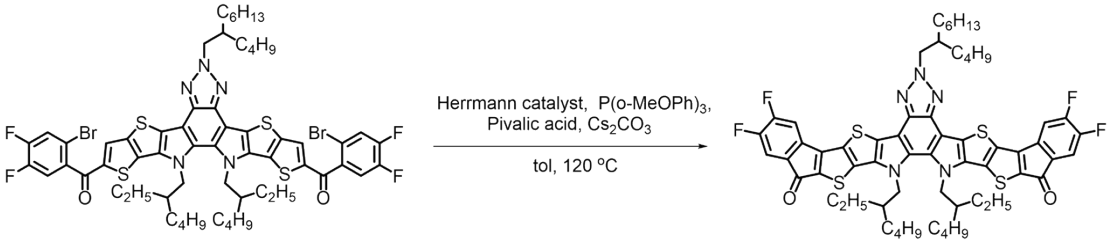

4 5

Compound 5: Under protection of argon, Herrmann catalyst (trans-bis(acetato)bis[*o*-(di-*o*-tolylphosphino)benzyl]dipalladium (II)) (3 mg, 0.003 mmol), P(o-MeOPh)$_3$ (2 mg, 0.006 mmol), Pivalic acid (17 mg, 0.17 mmol), Cs_2CO_3 (164 mg, 0.50 mmol) was added to a solution of compound 4 (210 mg，0.17 mmol) in 7.0 mL toluene. The mixture was heated to 120 °C and stirred for 32 hours. Then removal of solvent, this crude product was purified by silica gel chromatography (petroleum ether/dichloromethane = 1.0:1.5, v/v) to afford compound 5 (188 mg, yield: 90%) as a

purple black solid. ^{1}H NMR (500 MHz, Chloroform-*d*) δ 7.43 – 7.37 (m, 1H), 7.18 – 7.13 (m, 1H), 4.76 (d, *J* = 7.0 Hz, 1H), 4.72 (d, *J* = 7.1 Hz, 1H), 4.65 (d, *J* = 7.7 Hz, 2H), 2.38 (s, 0.5H), 2.00 – 1.90 (m, 1H), 1.42 – 1.23 (m, 8H), 1.04 – 0.74 (m, 11H), 0.72 – 0.50 (m, 6H). ^{13}C NMR (126 MHz, Chloroform-d) δ 182.42, 152.23, 148.98, 136.76, 136.32, 135.72, 134.92, 134.67, 133.01, 132.39, 127.56, 114.43, 114.27, 111.05, 110.48, 110.31, 59.91, 55.11, 40.26, 39.08, 31.79, 31.10, 29.58, 28.42, 27.62, 26.13, 23.18, 22.92, 22.68, 22.66, 22.63, 14.04, 13.67, 13.64, 10.23, 10.08.

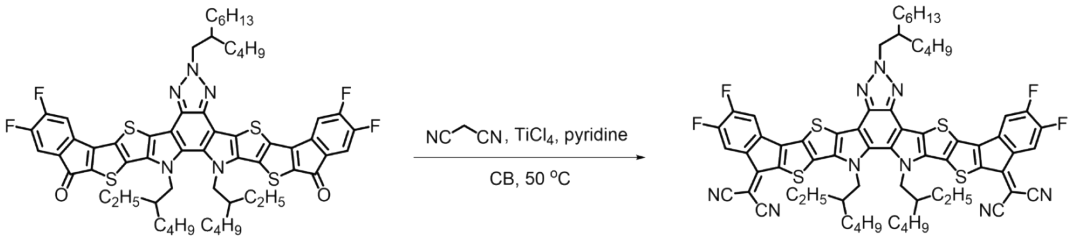

5 FM4

Compound FM4: To a stirred solution of compound 5 (166 mg, 0.15 mmol) and malononitrile (50 mg, 0.76 mmol) in 20.0 mL chlorobenzene was added 0.2 mL pyridine and 0.2 mL $TiCl_4$, the solution was heated to 50 °C for 4 hours. Then the solution was poured into water and extracted with CH_2Cl_2, the organic layer was washed with water and brine, and was dried over Na_2SO_4, after removal of solvent, this crude product was purified by silica gel chromatography (petroleum ether/dichloromethane = 1.0:1.5, v/v) to afford compound FM4 (140 mg, yield: 78%) as a black solid. ^{1}H NMR (500 MHz, Chloroform-d) δ 8.11 – 8.05 (m, 1H), 7.23 (s, 1H), 4.76 (d, J = 7.0 Hz, 1H), 4.72 (d, J = 7.1 Hz, 1H), 4.65 (d, J = 7.7 Hz, 2H), 2.38 (s, 0.5H), 2.00 - 1.90 (m, 1H), 1.42-1.23 (m, 8H), 1.04 – 0.74 (m, 11H), 0.72 – 0.50 (m, 6H). ^{13}C NMR (126 MHz, Chloroform-d) δ 154.74, 151.78, 149.19, 144.90, 137.41, 137.26, 135.69, 134.56, 134.53, 133.75, 132.95, 128.79, 116.86, 116.69, 113.92, 112.99, 111.87, 111.28, 111.11, 59.98, 55.41, 40.31, 39.09, 31.78, 31.43, 31.09, 29.57, 28.41, 27.60, 26.13, 23.25, 22.91, 22.63, 14.12, 14.03, 13.65, 10.16, 0.00. MS (MALDI-TOF): Calculated for $C_{66}H_{63}F_4N_9S_4$ [M^+], 1185.4; found, 1185.4.

3. Thermal properties

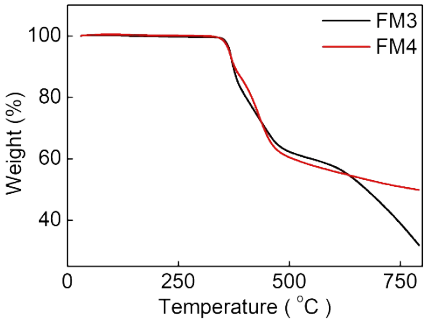

Figure S1. TGA curve of FM3 and FM4 under N_2 atmosphere at a scan rate of 10 °C min^{-1}. The T_d of FM3 and FM4 are 364 °C and 362 °C, respectively.

4. Density functional theory calculations

Figure S2. Side view of the geometry-optimized structure for the model molecules of (a) FM3 and (b) FM4 with all the long alkyl chains being replaced by methyl groups for simplification.

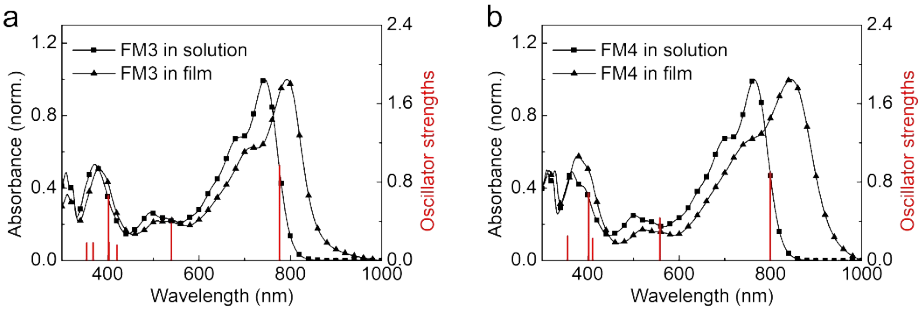

Figure S3. UV-vis absorption spectra of (a) FM3 and (b) FM4 in solution and in thin film. The red bars show the transition energies and oscillator strengths simulated by TD-DFT calculations.

Excitation energies and oscillator strengths of FM3 (Oscillator strength exceeding 0.1):

Excited State 1: Energy: 1.5975 eV, Wavelength: 776.13 nm, Oscillator strength: 0.9677, Configulations: HOMO-1 → LUMO+1 (-0.11770), HOMO → LUMO (0.68972);

Excited State 4: Energy: 2.2985 eV, Wavelength: 539.42 nm, Oscillator strength:

0.3747, Configulations: HOMO-3 → LUMO (-0.40515), HOMO-1 → LUMO+1 (0.53630), HOMO → LUMO (0.15743);

Excited State 10: Energy: 3.0784 eV, Wavelength: 402.76 nm, Oscillator strength: 0.1877, Configulations: HOMO-7 → LUMO (-0.13652), HOMO-5 → LUMO+1 (0.16381), HOMO-4 → LUMO (-0.64541), HOMO-2 → LUMO (0.14447);

Excited State 11: Energy: 3.0839 eV, Wavelength: 402.04 nm, Oscillator strength: 0.6608, Configulations: HOMO-6 → LUMO (-0.14980), HOMO-5 → LUMO (0.13294), HOMO-4 → LUMO+1 (0.21231), HOMO → LUMO+2 (0.63337);

Excited State 14: Energy: 3.3684 eV, Wavelength: 368.08 nm, Oscillator strength: 0.1817, Configulations: HOMO-8 → LUMO+1 (-0.14443), HOMO-7 → LUMO (0.61655), HOMO-5 → LUMO+1 (-0.16009), HOMO-4 → LUMO (-0.17302);

Excited State 16: Energy: 3.4958 eV, Wavelength: 354.66 nm, Oscillator strength: 0.1798, Configulations: HOMO-7 → LUMO (-0.15974), HOMO-6 → LUMO+1 (0.63901), HOMO-5 → LUMO+1 (-0.22191).

Excitation energies and oscillator strengths of FM4 (Oscillator strength exceeding 0.1):

Excited State 1: Energy: 1.5517 eV, Wavelength: 799.02 nm, Oscillator strength: 0.8999, Configulations: HOMO-1 → LUMO+1 (0.13509), HOMO → LUMO (-0.68466);

Excited State 4: Energy: 2.2234 eV, Wavelength: 557.63 nm, Oscillator strength: 0.4353, Configulations: HOMO-3 → LUMO (0.41308), HOMO-1 → LUMO+1 (-0.52454), HOMO → LUMO (-0.18117);

Excited State 10: Energy: 3.0178 eV, Wavelength: 410.84 nm, Oscillator strength: 0.2286, Configulations: HOMO-7 → LUMO (0.11736), HOMO-4 → LUMO (-0.66575), HOMO-2 → LUMO (0.12644);

Excited State 11: Energy: 3.0801 eV, Wavelength: 402.54 nm, Oscillator strength: 0.6922, Configulations: HOMO-6 → LUMO (-0.13028), HOMO-4 → LUMO+1 (-0.31660), HOMO → LUMO+2 (0.60485);

Excited State 16: Energy: 3.4832 eV, Wavelength: 355.95 nm, Oscillator strength: 0.2501, Configulations: HOMO-8 → LUMO (0.17480), HOMO-6 → LUMO+1 (-0.65146), HOMO-5 → LUMO+1 (0.10423).

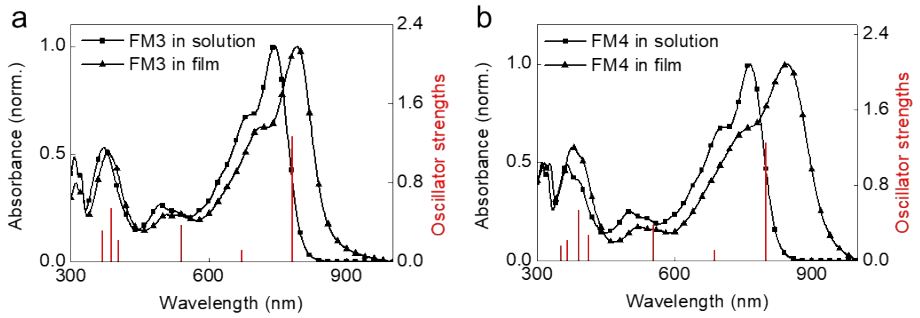

Figure S4. UV-vis absorption spectra of (a) FM3 and (b) FM4 in solution and in thin film. The red bars show the transition energies and oscillator strengths simulated by TD-DFT calculations with chloroform as solvent.

Excitation energies and oscillator strengths of FM3 (chloroform as solvent) (Oscillator strength exceeding 0.1):

Excited State 1: Energy: 1.5843 eV, Wavelength: 782.56 nm, Oscillator strength: 1.2708, Configulations: HOMO → LUMO (0.69526);

Excited State 2: Energy: 1.8430 eV, Wavelength: 672.72 nm, Oscillator strength: 0.1213, Configulations: HOMO-1 → LUMO (-0.12398), HOMO → LUMO+1 (0.67926);

Excited State 5: Energy: 2.2916 eV, Wavelength: 541.04 nm, Oscillator strength: 0.3664, Configulations: HOMO-3 → LUMO (-0.38741), HOMO-2 → LUMO+1 (-0.16531), HOMO-1 → LUMO+1 (0.54717), HOMO → LUMO (0.10836);

Excited State 10: Energy: 3.0678 eV, Wavelength: 404.14 nm, Oscillator strength: 0.2178, Configulations: HOMO-7 → LUMO (-0.10132), HOMO-5 → LUMO+1 (-0.18698), HOMO-4 → LUMO (0.64656), HOMO-2 → LUMO (0.12645);

Excited State 11: Energy: 3.1897 eV, Wavelength: 388.71 nm, Oscillator strength: 0.5397, Configulations: HOMO-6 → LUMO (-0.24304), HOMO-5 → LUMO (-0.12724), HOMO-4 → LUMO+1 (-0.32104), HOMO → LUMO+2 (0.55497);

Excited State 14: Energy: 3.3609 eV, Wavelength: 368.90 nm, Oscillator strength: 0.3195, Configulations: HOMO-8 → LUMO+1 (-0.15554), HOMO-7 → LUMO (0.60534), HOMO-6 → LUMO+1 (0.20093), HOMO-5 →LUMO+1 (0.13937), HOMO-4 →LUMO (0.13438).

Excitation energies and oscillator strengths of FM4 (chloroform as solvent)

(Oscillator strength exceeding 0.1):

Excited State 1: Energy: 1.5501 eV, Wavelength: 799.84 nm, Oscillator strength: 1.2496, Configulations: HOMO → LUMO (0.69447);

Excited State 2: Energy: 1.8048 eV, Wavelength: 686.99 nm, Oscillator strength: 0.1128, Configulations: HOMO-3 → LUMO+1 (0.10895), HOMO-1 → LUMO (-0.13690), HOMO → LUMO+1 (0.67481);

Excited State 5: Energy: 2.2383 eV, Wavelength: 553.91 nm, Oscillator strength: 0.3781, Configulations: HOMO-3 → LUMO (-0.38341), HOMO-2 → LUMO+1 (-0.16600), HOMO-1 → LUMO+1 (0.55177), HOMO → LUMO (0.11331);

Excited State 10: Energy: 3.0122 eV, Wavelength: 411.60 nm, Oscillator strength: 0.2686, Configulations: HOMO-5 → LUMO+1 (0.17957), HOMO-4 → LUMO (0.65583), HOMO-2 → LUMO (-0.12532);

Excited State 12: Energy: 3.1741 eV, Wavelength: 390.61 nm, Oscillator strength: 0.5396, Configulations: HOMO-6 → LUMO (0.16432), HOMO-4 → LUMO+1 (0.44502), HOMO → LUMO+2 (0.49695);

Excited State 14: Energy: 3.3920 eV, Wavelength: 365.52 nm, Oscillator strength: 0.2196, Configulations: HOMO-9 → LUMO+1 (0.15946), HOMO-7 → LUMO (0.62766), HOMO-5 → LUMO+1 (-0.17529), HOMO-4 → LUMO (0.12734);

Excited State 15: Energy: 3.3955 eV, Wavelength: 365.14 nm, Oscillator strength: 0.1218, Configulations: HOMO-6 → LUMO (-0.42437), HOMO-4 → LUMO+1 (-0.31543), HOMO → LUMO+2 (0.43803);

Excited State 17: Energy: 3.5087 eV, Wavelength: 353.36 nm, Oscillator strength: 0.1591, Configulations: HOMO-8 → LUMO (-0.42487), HOMO-7 → LUMO (-0.12649), HOMO-6 → LUMO+1 (0.51260), HOMO-5 → LUMO+1 (0.13582).

5. The photoluminescence (PL) measurements

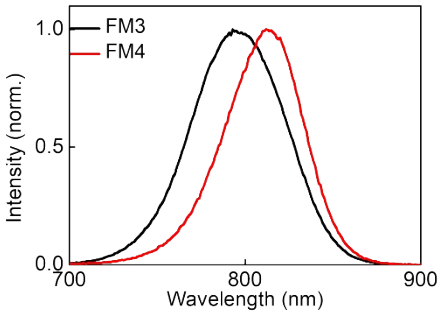

Figure S5. The fluorescence spectra of FM3 and FM4 in chloroform solution.

We also tested the fluorescence quantum efficiency of FM4 and Y6 films. The fluorescence quantum efficiency is 0.1% for FM4 film and 0.7% for Y6 film. The fluorescence quantum efficiency of FM4 is lower than that of Y6. This may result in higher non-radiated energy losses and voltage losses for FM4-based devices.

6. The light and chemical stability

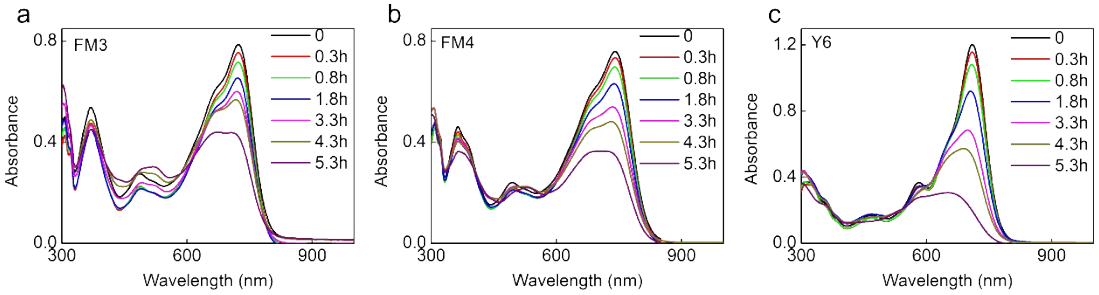

Figure S6. The UV-vis absorption spectra of (a) FM3, (b) FM4 and (c) Y6 under 100 mW cm^{-2} AM 1.5 G simulated solar light for different time.

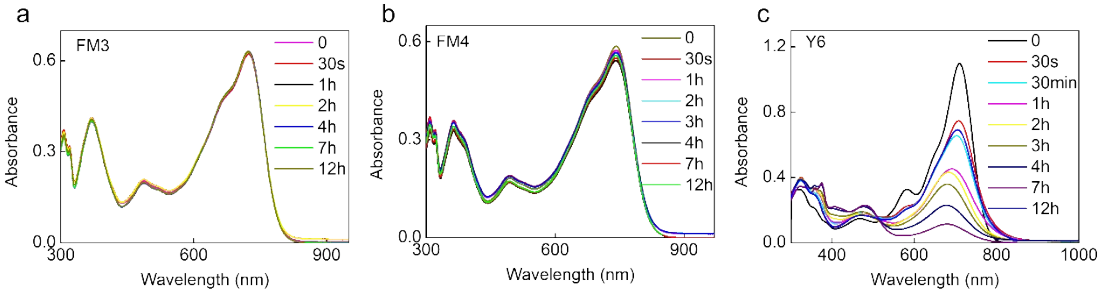

Figure S7. The UV-vis absorption spectra of (a) FM3, (b) FM4 and (c) Y6 treated in the diluted THF solution (10^{-5} mol L^{-1}) with 100 equiv ethanolamine for different time.

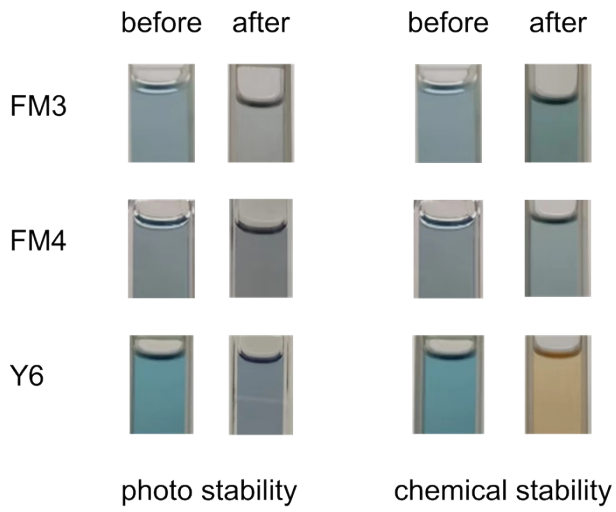

Figure S8. The color variation of the FM3, FM4 and Y6 solutions before and after irradiation for 5.3 h (photo stability), and before and after addition of ethanolamine for 12 h (chemical stability).

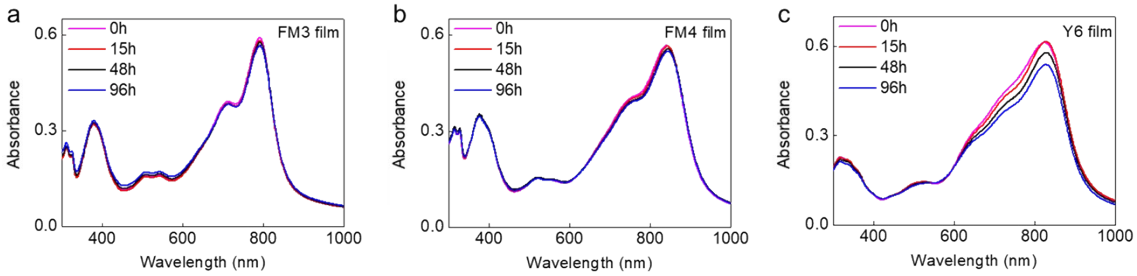

Figure S9. The absorption spectra of (a) FM3, (b) FM4 and (c) Y6 films under 100 mW cm^{-2} AM 1.5 G simulated solar light for different time.

Both FM3 and FM4 films exhibited almost constant absorption spectra during 96 hours of illumination. As a comparison, Y6 film exhibited varied absorption spectra with a 13% reduction in the intensity of the maximum absorption peak after the 96 hours irradiation. These results suggest that both FM3 and FM4 films have better photo stability than that of Y6 film.

7. The stacking properties of the materials

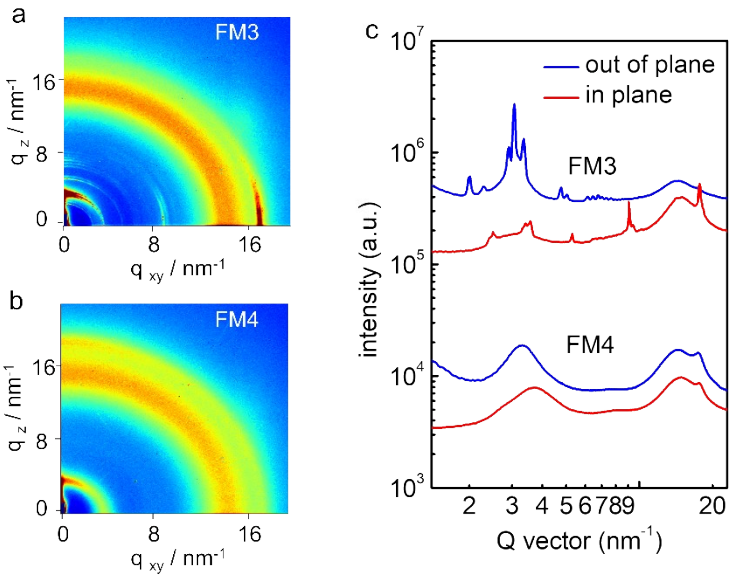

Figure S10. 2D GIWAXS images of (a) FM3 and (b) FM4. (c) 1D line cuts of the corresponding 2D-GIWXAS patterns of FM3 and FM4 along the in-plane and out-of-plane directions.

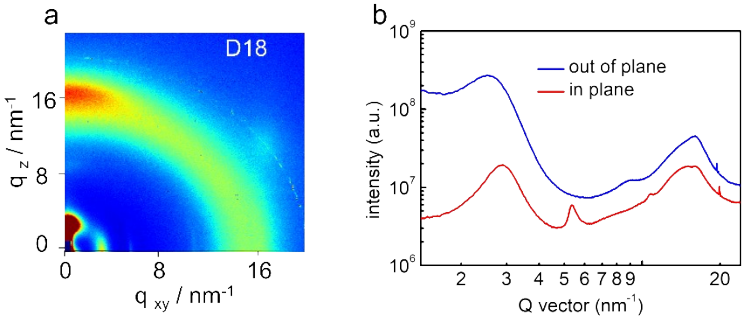

Figures S11. (a) 2D-GIWAXS patterns of the neat film of D18. (b) 1D line cuts of the corresponding 2D-GIWXAS patterns of D18 along the in-plane and out-of-plane directions.

Table S1. GIWAXS characterization data of the FM3, FM4, D18, D18:FM3 and D18:FM4 films.

Films	Directions	100				010			
		Location [nm^{-1}]	d-spacing [Å]	FWHM [Å^{-1}]	CL [Å]	Location [nm^{-1}]	d-spacing [Å]	FWHM [Å^{-1}]	CL [Å]
FM3	Out-of-plane	3.07	20.46	0.01	669.67				
	In-plane	3.56	17.64	0.07	81.83	17.72	3.55	0.05	124.22
FM4	Out-of-plane	3.29	19.09	0.01	57.09	17.63	3.56	0.20	27.98
	In-plane	3.69	17.02	0.14	40.66	17.79	3.55	0.23	25.06

D18	Out-of-plane	2.53	24.82	0.11	53.32	16.00	3.92	0.46	12.33
	In-plane	2.87	21.89	0.09	62.11	16.00	3.92	0.33	17.36
D18:FM3	Out-of-plane	2.84	22.11	0.11	53.83	16.37	3.84	0.28	20.19
	In-plane	2.91	21.85	0.07	84.36	17.67	3.55	0.17	34.25
D18:FM4	Out-of-plane					16.40	3.82	0.24	23.95
	In-plane	2.94	21.36	0.07	81.91				

8. OSC devices fabrication and measurement

The OSC devices were fabricated with the structure of ITO/ZnO/active layer/MoO_3/Al. ITO glass substrates were cleaned in an ultrasonic bath with deionized water, acetone, and isopropyl alcohol, and then dried at 125 °C for 30 min. After treated with ultraviolet–ozone for 15 min, ZnO layers (ca. 30 nm) was spin-coated at 5000 rpm onto the cleaned ITO glasses from ZnO precursor solution, and then baked at 200 °C for 60 min in air. The ZnO precursor was synthesized by dissolving zinc acetate dehydrate (200 mg) and ethanolamine (65 mg) in 2 mL 2-methoxyethanol under vigorous stirring for 10 h in air. All of the substrates were placed into a nitrogen-filled glove box. Subsequently, D18:FM4 (1:1.4 weight ratio) based blends were dissolved in CF with a concentration of 10.0 mg/mL. The solutions were stirred at 55 °C for 2 h and 80 °C for 2h, then adding 0.5% CN and stirred for 30 min and then spin-coated onto the substrates at room temperature to obtain the active layers. After drying for 40min, the active layers were thermal annealed at 110 °C for 10 min. Then, the device fabrication was completed by thermally evaporating MoO_3 (15 nm) and aluminum (100 nm) under vacuum at a pressure of 2×10^{-4} Pa. The active area of the devices, defined by a shadow mask, was 2 mm^2. The current density (*J*–*V*) curves of the OSC devices were measured using a computer-controlled Keithley 2400 sourcemeter under 100 mW cm^{-2} AM 1.5G simulated solar light illumination. An XES-40S2-CE class solar simulator (Japan, SAN-EI Electric Co., Ltd) was used to provide the AM 1.5G simulated solar light illumination.

Table S2. Photovoltaic performance of D18:FM4-based solar cells with thermal annealing treatments at various temperatures.

Temperature (℃)	V_{oc} (V)	J_{sc} (mA cm^{-2})	FF (%)	PCE (%)
110	0.74	19.26	57.8	8.24

150	0.72	20.46	52.5	7.74
180	0.73	18.35	55.4	7.42

Table S3. Photovoltaic performance of D18:FM4-based solar cells with different device structures.

Device structure	V_{oc} (V)	J_{sc} (mA cm^{-2})	FF (%)	PCE (%)
conventional	0.74	19.26	57.8	8.24
inverted	0.73	19.60	58.8	8.41

Table S4. Photovoltaic performance of D18:FM4-based solar cells with different dosages of 1-CN.

1-CN	V_{oc} (V)	J_{sc} (mA cm^{-2})	FF (%)	PCE (%)
As-cast	0.73	19.60	58.8	8.41
0.5% CN	0.73	20.88	61.4	9.35
1.0% CN	0.71	19.07	67.7	9.17
2.0% CN	0.69	13.18	63.0	5.73

Table S5. Photovoltaic performance of D18:FM4-based solar cells with different molecular weights of D18.

*M*n of D18 (*k*Da)	V_{oc} (V)	J_{sc} (mA cm^{-2})	FF (%)	PCE (%)
20.8	0.73	9.03	43.6	2.87
68.7	0.72	21.58	65.1	10.12
70~80	0.73	20.88	61.4	9.35
150.0	0.71	18.72	66.0	8.77

Table S6. Photovoltaic performance of D18:FM4-based solar cells with different ratios of donor and acceptor.

Donor: Acceptor	V_{oc} (V)	J_{sc} (mA cm^{-2})	FF (%)	PCE (%)
1:1.2	0.72	21.58	65.1	10.12
1:1.4	0.72	21.18	67.2	10.25

1:1.6	0.72	21.01	66.9	10.13
1:2.0	0.72	20.73	61.8	9.22

Table S7. Photovoltaic performance of D18:FM4-based solar cells with different rotate speeds.

n (r)	V_{oc} (V)	J_{sc} (mA cm^{-2})	FF (%)	PCE (%)
3000	0.71	21.82	63.5	9.83
3700	0.72	21.18	67.2	10.25
4500	0.72	20.73	66.8	9.97
5500	0.72	21.18	66.6	10.15

Table S8. Photovoltaic performance of D18:FM3-based solar cells.

	V_{OC} (V)	J_{SC} (mA/cm^2)	FF	PCE (%)
1	0.82	4.42	0.39	1.41
2	0.83	4.11	0.37	1.26
3	0.83	5.15	0.40	1.71
4	0.82	5.31	0.41	1.79
5	0.83	3.91	0.39	1.27
6	0.83	3.87	0.38	1.22
7	0.82	3.89	0.39	1.24
8	0.83	3.45	0.38	1.09
9	0.82	4.78	0.46	1.80
10	0.81	5.26	0.42	1.79

Table S9. Photovoltaic performance of D18:FM4-based solar cells.

	V_{OC} (V)	J_{SC} (mA/cm^2)	FF	PCE (%)
1	0.68	23.11	0.70	10.94
2	0.68	23.70	0.68	11.05
3	0.68	23.64	0.70	11.00
4	0.68	23.55	0.68	11.24
5	0.68	23.52	0.69	10.93
6	0.68	23.64	0.68	11.02
7	0.68	23.58	0.70	10.96
8	0.68	23.11	0.69	10.97
9	0.68	23.40	0.70	10.91
10	0.68	23.97	0.70	11.36

9. Hole/electron-only devices fabrication and hole/electron mobility measurement

The hole/electron mobilities were measured using the space charge limited current (SCLC) method. The electron-only device structure for the FM3 or FM4 film is ITO/ PEIE/FM3 or FM4/Ca/Al. The hole-only and electron-only device structures for the active layers are ITO/PEDOT: PSS/active layer/MoO_3/Al and ITO/PEIE/active layer/Ca/Al, respectively. The current-voltage curves in the range of 0–8 V were recorded using a computer-controlled Keithley 2400 source meter, and the results were fitted to a space-charge limited function:

$$J = \frac{9}{8}\varepsilon_r\varepsilon_0\mu\frac{V^2}{L^3}\exp\left(0.89\beta\frac{\sqrt{V}}{\sqrt{L}}\right)$$

where J is the current density, ε_0 is the permittivity of free space, ε_r is the relative permittivity of 3 for molecules, μ is the zero-field mobility, V is the potential across the device ($V = V_{applied} - V_{bias} - V_{series}$), L is the thickness of active layer, and β is the field-activation factor. The series and contact resistance (V_{series}) of the device (10–15 Ω) were measured using blank device of ITO/PEDOT:PSS/MoO_3/Al or ITO/PEIE/Ca/Al. The range of 0–5 V was used to extract the mobility values.

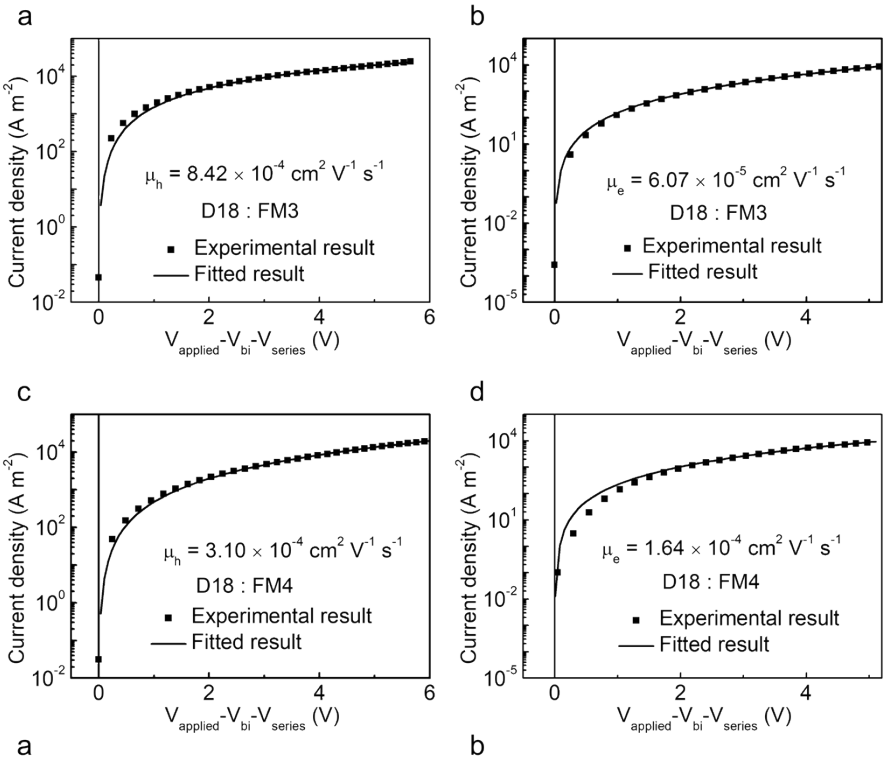

Figure S12. *J–V* curves and SCLC fittings (a, c) the hole-only devices and (b, d) the electron-only devices based on D18:FM3 and D18:FM4 blends, respectively.

10. Charge generation, collection and recombination behaviors

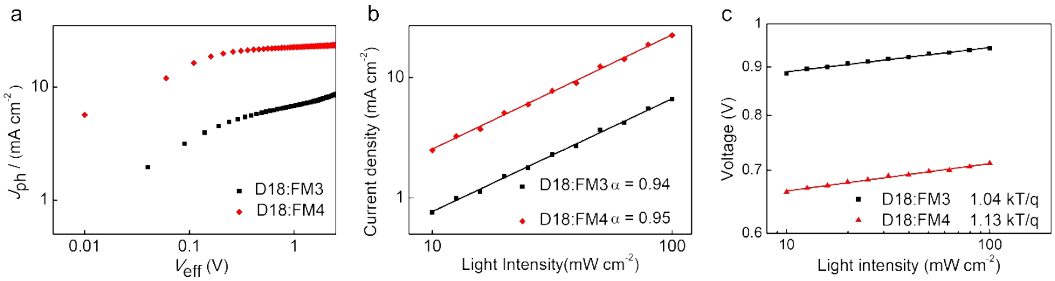

Figure S13. (a) J_{ph} versus V_{eff} plots; (b) dependence of J_{SC} on light intensity and (c) dependence of V_{OC} on light intensity for OSCs based on D18:FM3 and D18:FM4 films.

The geminate recombination behaviors of the two OSC devices based on D18:FM3 and D18:FM4 were investigated by measuring the dependence of V_{OC} on the light density (P). The relationship between V_{OC} and P can be described by the formula $V_{OC} \propto \ln P$, nk_BT/q is slope of the formula, where k_B is the Boltzmann constant, T is temperature, and q is the elementary charge. When n is equal to 2, trap-assisted recombination dominates in the device; When n is equal to 1, bimolecular recombination dominates in the device. As shown in Fig. S13c, the slopes of D18:FM3

and D18:FM4-based devices are 1.04 k_BT/q and 1.13 k_BT/q, respectively, suggesting trap-assisted recombination is suppressed and bimolecular recombination dominates in the two devices.

11. The stability of OSC devices

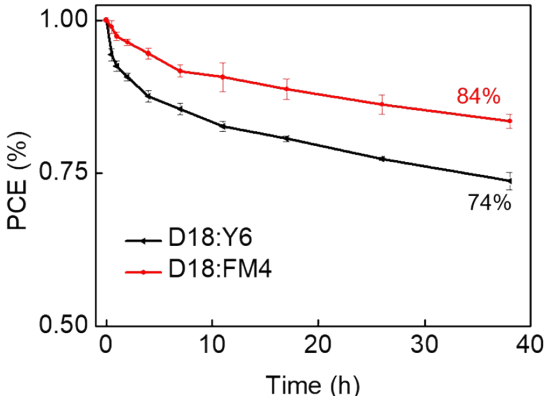

Figure S14. The PCE values of the inverted OSC devices based on D18:FM4 and D18:Y6 active layers after illumination under 100 mW cm^{-2} AM 1.5 G simulated solar light for different time. The error bars with average values were obtained from five individual devices.

Table S10. Photovoltaic parameters of the OSC devices based on D18:FM4 blend under illumination of AM 1.5 G, 100 mW cm^{-2} with different time.

Test time (h)	V_{OC} (V)	J_{SC} (mA/cm^2)	FF	PCE (%)[a]
0	0.72 ± 0.00	20.99 ± 0.26	0.67 ± 0.56	10.10 ± 0.07
0.5	0.69 ± 0.01	20.99 ± 0.31	0.69 ± 0.73	10.00 ± 0.14
1	0.68 ± 0.01	20.93 ± 0.28	0.69 ± 0.53	9.84 ± 0.05
2	0.68 ± 0.00	20.87 ± 0.30	0.69 ± 0.38	9.74 ± 0.07
4	0.68 ± 0.01	20.85 ± 0.40	0.68 ± 0.85	9.56 ± 0.15
7	0.68 ± 0.01	20.38 ± 0.31	0.67 ± 0.59	9.26 ± 0.07
11	0.68 ± 0.01	20.51 ± 0.61	0.66 ± 0.77	9.15 ± 0.27
17	0.67 ± 0.00	20.31 ± 0.40	0.66 ± 0.63	8.97 ± 0.19
26	0.67 ± 0.01	20.05 ± 0.48	0.65 ± 0.90	8.70 ± 0.19
38	0.66 ± 0.01	20.10 ± 0.35	0.64 ± 0.78	8.46 ± 0.16

[a] The PCE values were obtained from five individual devices.

Table S11. Photovoltaic parameters of the OSC devices based on D18:Y6 blend under illumination of AM 1.5 G, 100 mW cm^{-2} with different time.

Test time (h)	V_{OC} (V)	J_{SC} (mA/cm^2)	FF	PCE (%) [a]
0	0.86 ± 0.01	24.00 ± 0.35	0.74 ± 0.63	15.36 ± 0.26
0.5	0.83 ± 0.01	23.83 ± 0.21	0.73 ± 0.84	14.50 ± 0.19

1	0.82 ± 0.00	23.88 ± 0.24	0.72 ± 0.69	14.21 ± 0.22
2	0.81 ± 0.01	23.71 ± 0.20	0.72 ± 0.50	13.94 ± 0.22
4	0.81 ± 0.01	23.42 ± 0.37	0.71 ± 0.83	13.44 ± 0.30
7	0.80 ± 0.00	23.22 ± 0.21	0.71 ± 0.60	13.13 ± 0.17
11	0.80 ± 0.01	23.04 ± 0.25	0.69 ± 0.56	12.62 ± 0.25
17	0.79 ± 0.00	22.84 ± 0.21	0.69 ± 0.90	12.44 ± 0.21
26	0.78 ± 0.01	22.20 ± 0.28	0.68 ± 0.79	11.89 ± 0.23
38	0.78 ± 0.01	22.09 ± 0.09	0.66 ± 0.62	11.37 ± 0.15

[a] The PCE values were obtained from five individual devices.

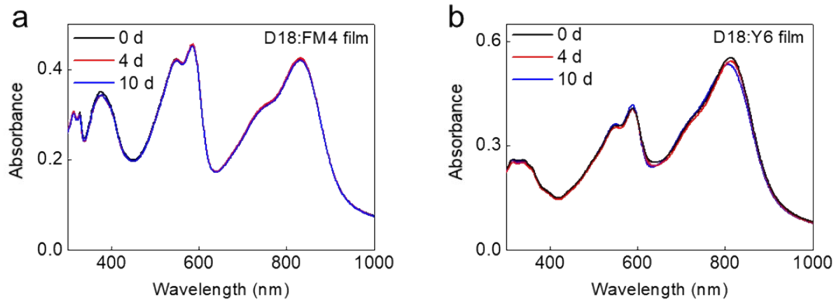

Figure S15. The absorption spectra of blend films of (a) D18:FM4 and (b) D18:Y6 on quartz substrates in humid environment (humidity: 60%~65%) for different time.

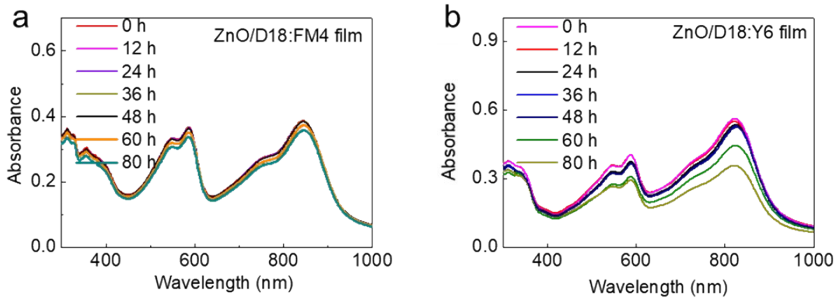

Figure S16. The absorption spectra of blend films of (a) D18:FM4 and (b) D18:Y6 on ZnO-coated quartz substrates in humid environment (humidity: 60%~65%) for different time.

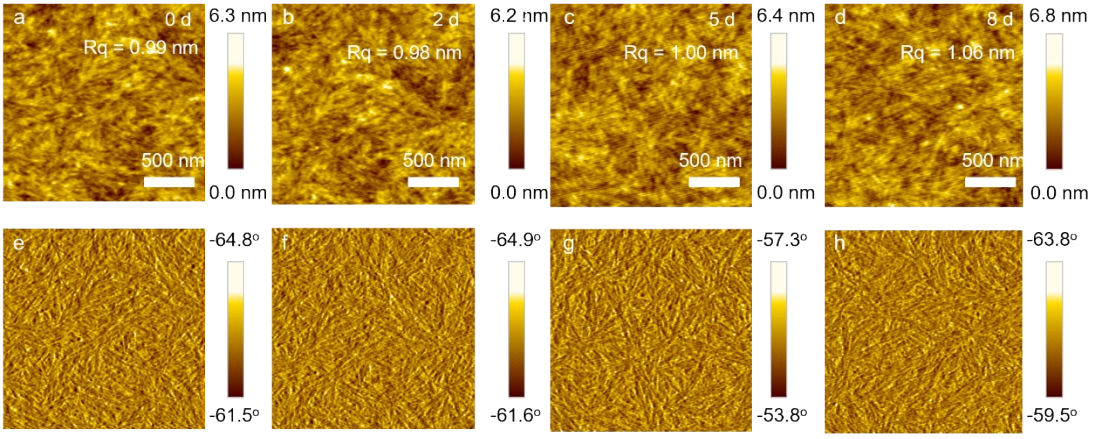

Figure S17. AFM (a, b, c and d) height images and (e, f, g and h) phase images of

D18:FM4 blend films after storaging in air for different time.

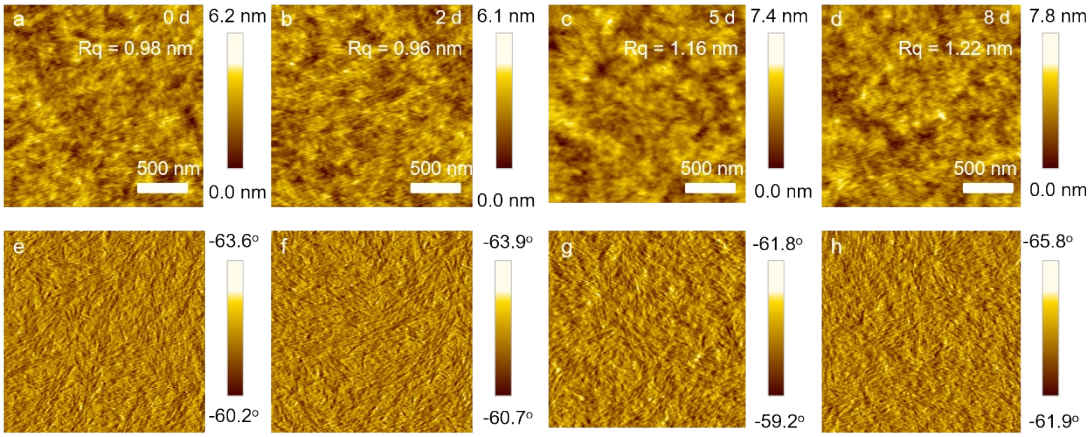

Figure S18. AFM (a, b, c and d) height images and (e, f, g and h) phase images of D18:Y6 blend films after storaging in air for different time.

In order to study the reason for the differences in air storage stability of the devices based on D18:FM4 and D18:Y6, we tested the degradation of the active films on quartz substrates or on ZnO-coated quartz substrates in humid environment (humidity: 60%~65%, accelerated aging test), as well as the morphology of the films in air (temperature: 18 °C~24 °C; humidity: 16%~25%) for different time. The degradation of active films was monitored by recording their absorption spectra, and the film morphology was investigated by atomic force microscopy (AFM). Figure S15 shows the absorption spectra of active films of D18:FM4 and D18:Y6 on quartz substrates with 60%~65% humidity for different times. The absorption spectra of D18:FM4 and D18:Y6 active films remained almost unchanged after storing for 10 days. This result indicates that the two blend films have similar wet tolerance. Figure S16 shows the absorption spectra of active films of D18:FM4 and D18:Y6 on ZnO-coated substrates with 60%~65% humidity for different times. D18:FM4 active film on ZnO-coated substrates exhibited a small variation in the absorption spectrum with maximum absorbance only decreased by 8.3% for 80 hours. In sharp contrast, the active film exhibited different absorption spectra with maximum absorbance decreased by 36.6% after 80 h of storing. This result indicates that in the presence of the ZnO interfacial layer, the degradation of D18:Y6 is significantly higher than that of D18:FM4. Figure S17 and S18 show AFM height and phase images of D18:FM4 and D18:Y6 active films

in air for different time, respectively. The surface morphology of both D18:FM4 and D18:Y6 films hardly changed in air for a long period. This indicates that the morphologic evolution is not the main reason for the insufficient air storage stability of device based on D18:Y6. The above results indicate that the degradation of the D18:Y6 active layer on ZnO-coated substrate contributes to the decrease in the air storage stability of the D18:Y6-based device. We speculate the diffusion of Zn ion from the ZnO layer to the interface of D18:Y6 active layer leads to degradation of the D18:Y6 active layer.[1]

12. ^{1}H NMR and ^{13}C NMR spectra

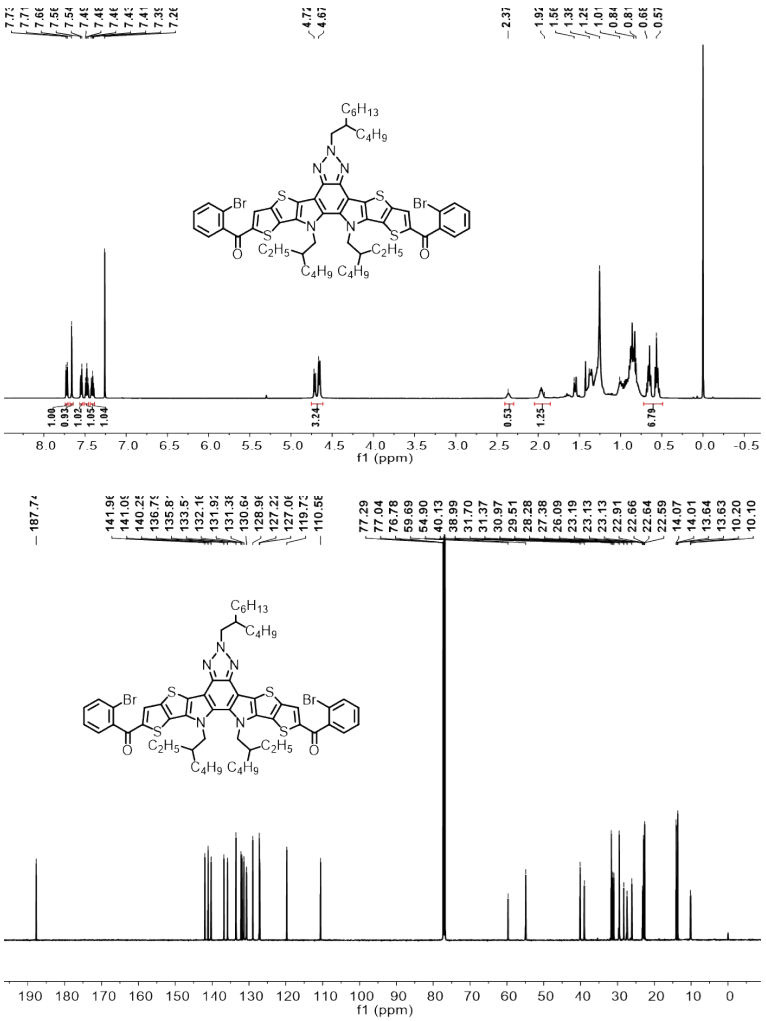

Figure S19. ^{1}H NMR and ^{13}C NMR of **2**.

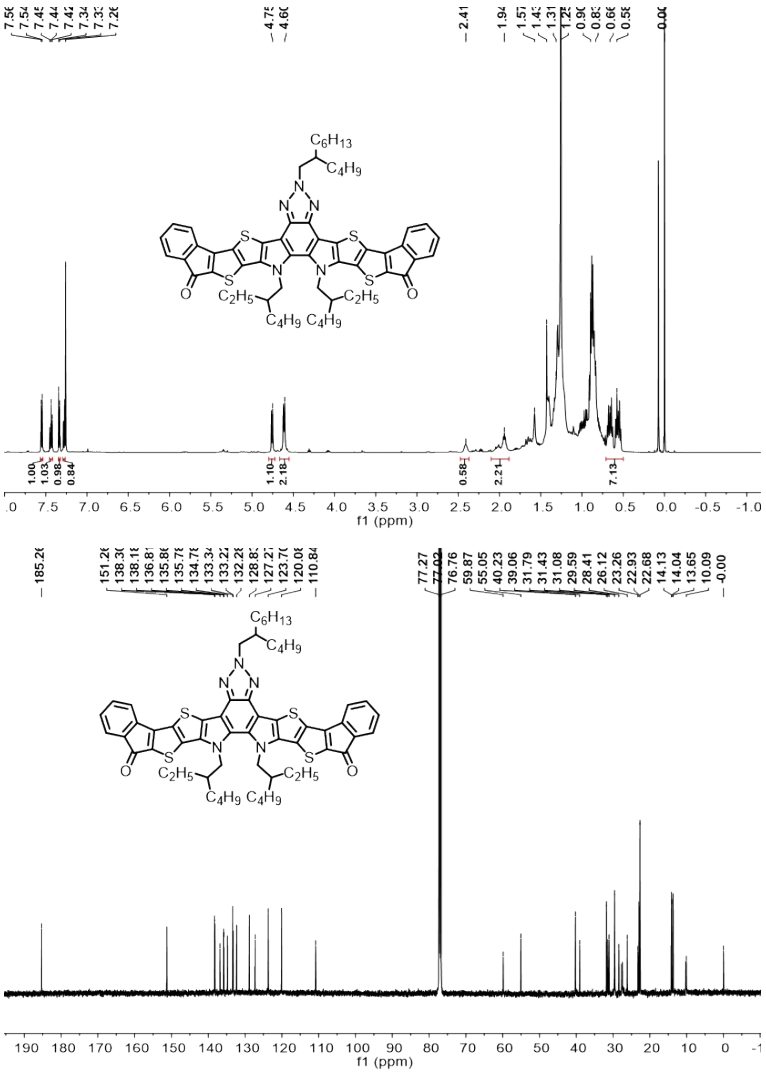

Figure S20. ^{1}H NMR and ^{13}C NMR of **3**.

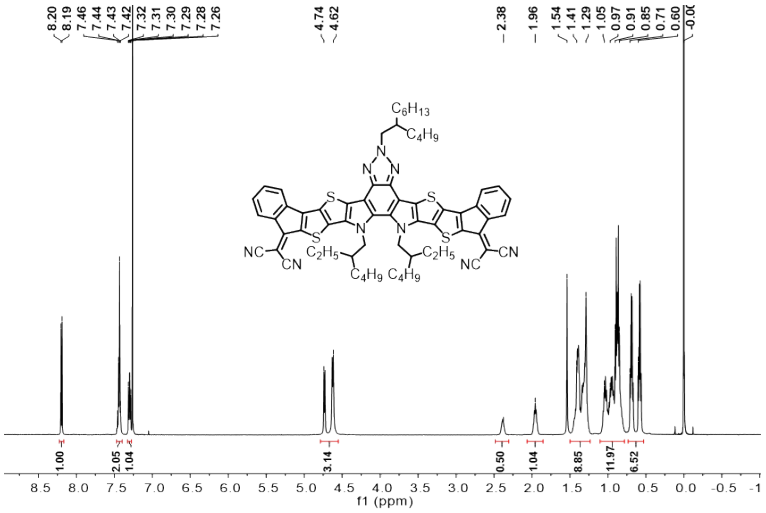

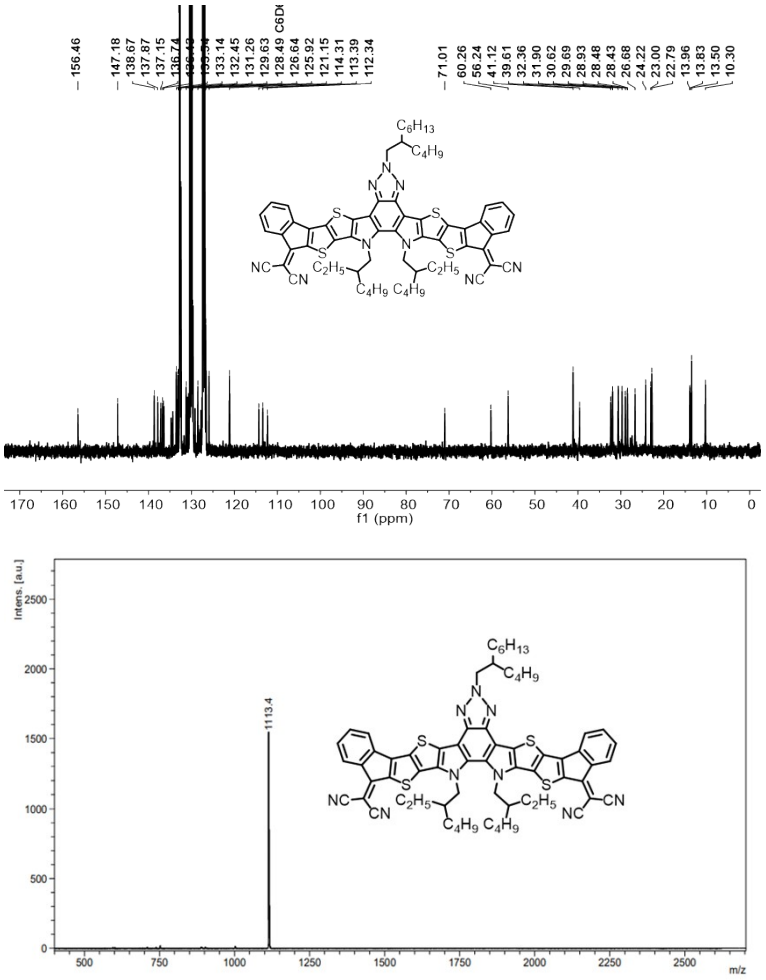

Figure S21. ^{1}H NMR, ^{13}C NMR and mass spectra of **FM3**.

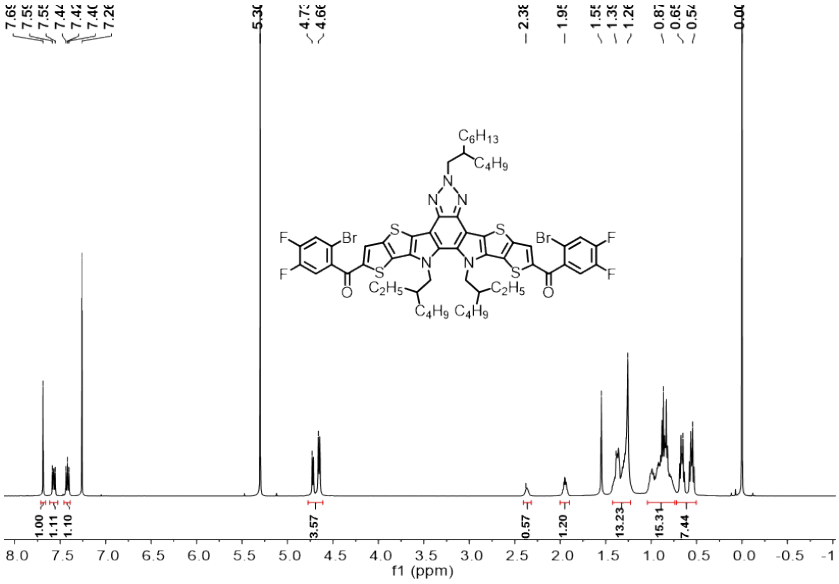

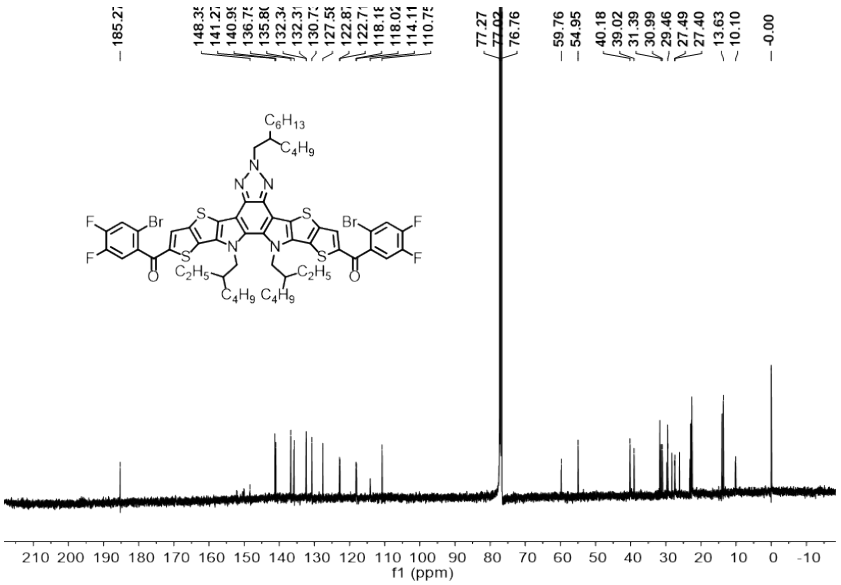

Figure S22. ^{1}H NMR and ^{13}C NMR of **4**.

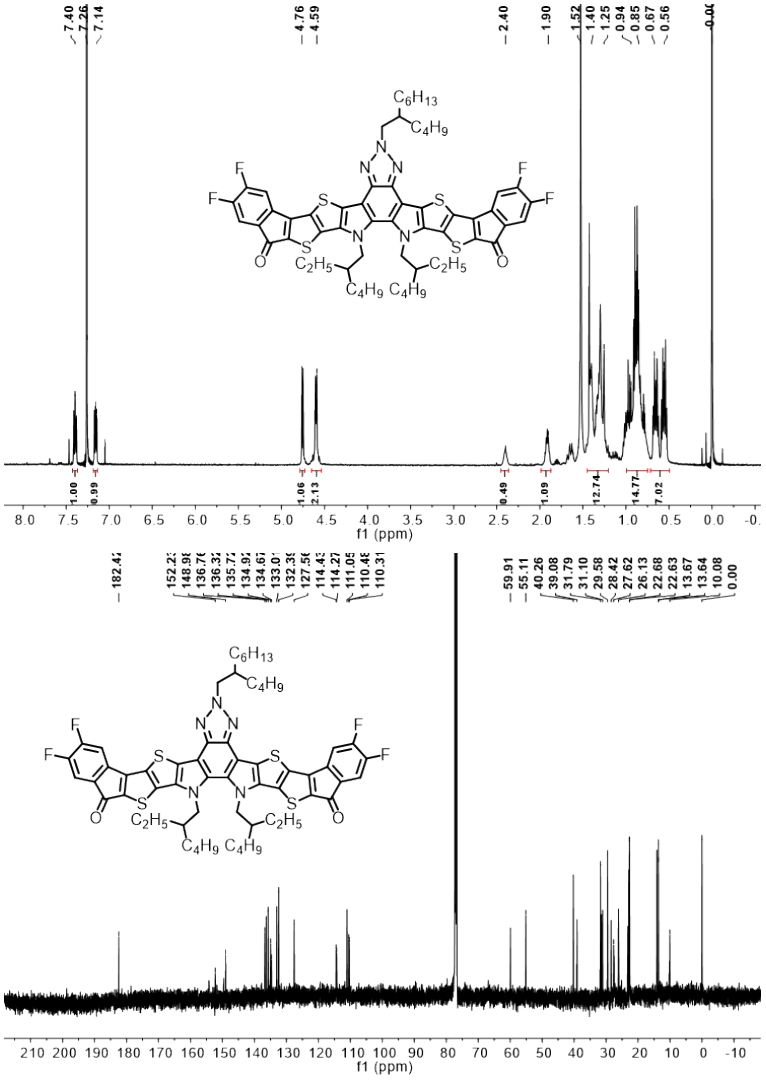

Figure S23. ^{1}H NMR and ^{13}C NMR of **5**.

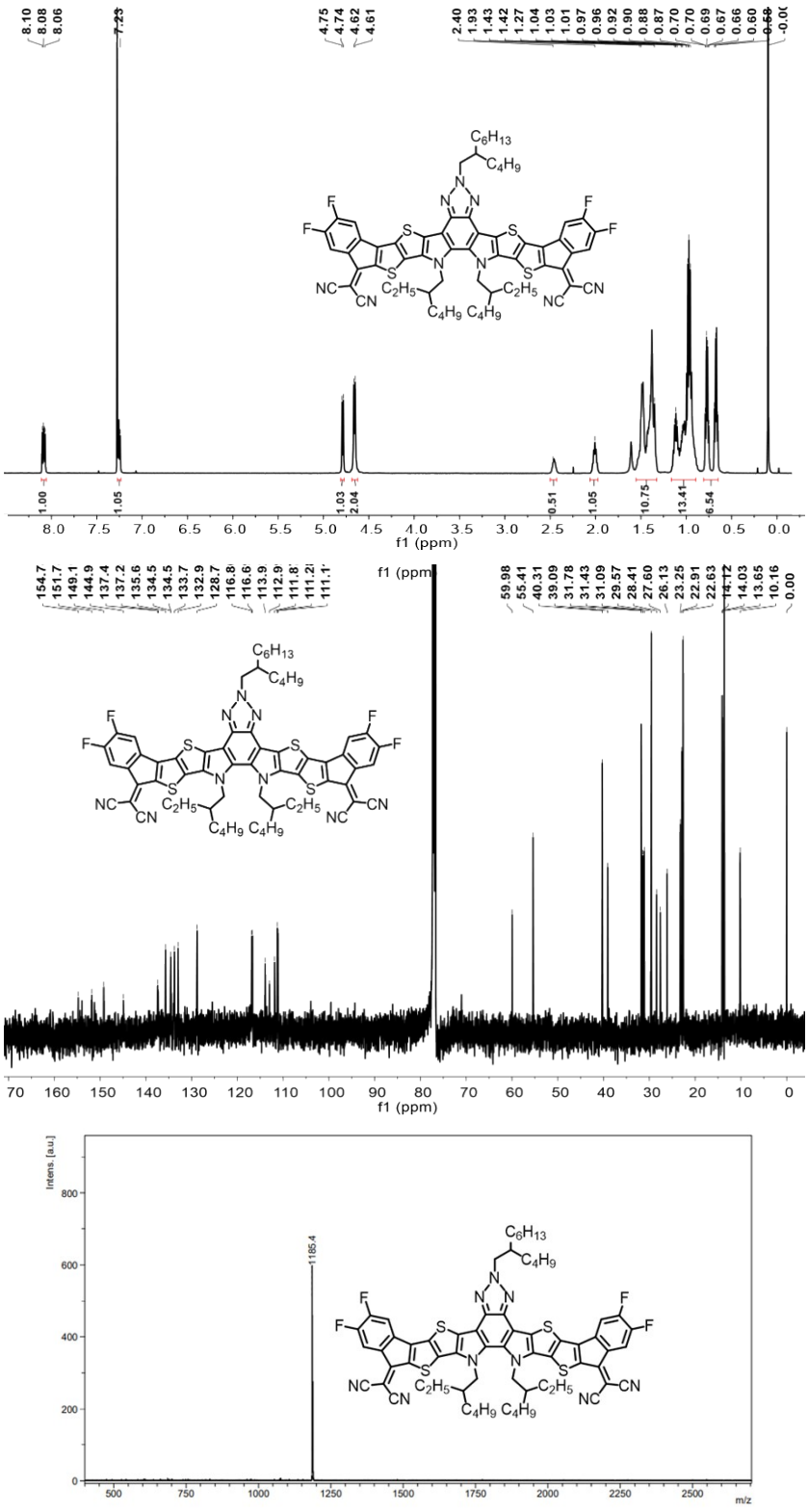

Figure S24. ^{1}H NMR, ^{13}C NMR and mass spectra of **FM4**.

13. Reference

1. S. Xiong, K. Fukuda, S. Lee, K. Nakano, X. Dong, T. Yokota, K. Tajima, Y. Zhou and T. Someya, *Adv. Sci.*, 2022, **9**, 2105288.